CHAPTER IV
RESULTS AND DISCUSSION

4.1 Characterization of Organically Modified MMT

After modification of MMT, sodium ions in the galleries of MMT were replaced by the quarternary ammonium ions of modifying agents and the organically modified MMT were characterized.

4.1.1 AAS

AAS was used to determine the amount of replaced Na^+ from washing water of modified MMT which assume to be equal to the amount of the modifying agents incorporated into MMT structure. The percentage of ion-exchange of the modified MMT was calculated by multiplying 100 with the ratio between replaced Na^+ determined by AAS and the total amount of Na^+ at the beginning. The calculated results were shown in Table 4.1.

Table 4.1 Na^+ exchanged percentage using two types of modifying agents

Modifying agent	Na^+ exchanged percentage
OC	94.70
OH	96.16

4.1.2 FT-IR

The incorporation of modifying agents into galleries of MMT could be verified using FT-IR. The FT-IR spectra of Na-MMT, modifying agents and organically modified MMTs are shown in Figures 4.1 and 4.2. For modifying agents, octadecylamine (OC) (see Figure 4.1) showed the important adsorption peaks of N-H stretching, C-H stretching of methyl and methylene group at 3300, 2950, 2850 and 1430 cm^{-1}, respectively. Di(hydrogenated tallow) dimethylammonium chloride (OH) (see Figure 4.2) showed the peaks of O-H stretching instead of N-H

stretching peak. FT-IR spectra of organically modified MMTs obtained combined the characteristic peaks of both inorganic Na-MMT and organic modifying agents.

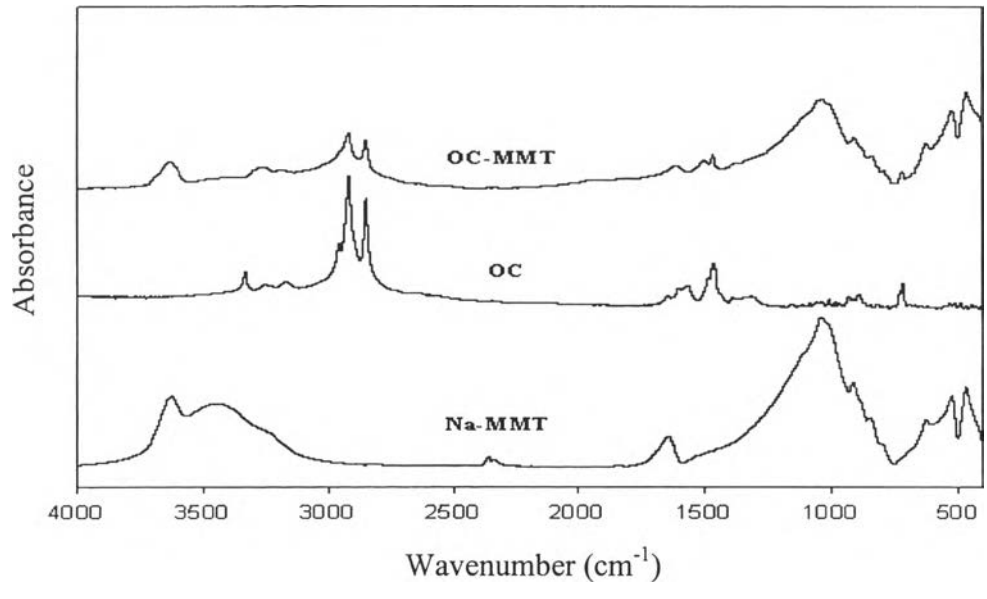

Figure 4.1 FT-IR spectra of Na-MMT, OC and OC-MMT.

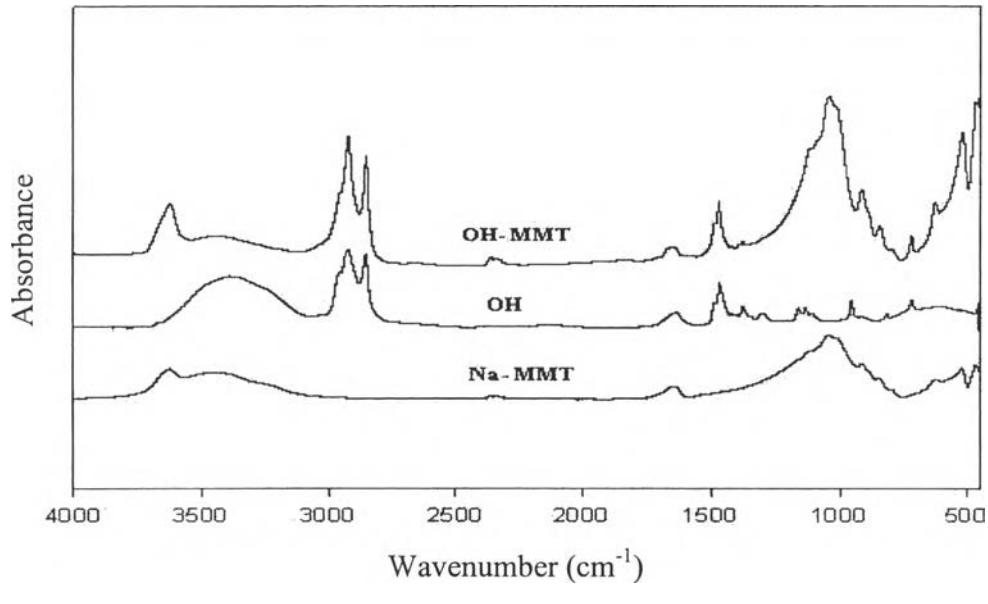

Figure 4.2 FT-IR spectra of Na-MMT, OH and OH-MMT.

4.1.3 XRD

As well as FT-IR, XRD also provided strongly evidence for the incorporation of modifying agents into the MMT structure. The XRD spectra of Na-

MMT and organically modified MMTs prepared using octadecylamine and di(hydrogenated tallow)dimethylammonium chloride as modifying agents were shown in Figure 4.3.

From Figure 4.3, the peak positions of both organically modified MMTs were shifted to lower degree relative to that of Na-MMT. This indicated that the spaces between the silicate layers were expanded significantly. This may be due to the incorporation of modifying agents into the galleries of MMT. The basal spacings calculated from the peak positions (2θ) were listed in Table 4.2.

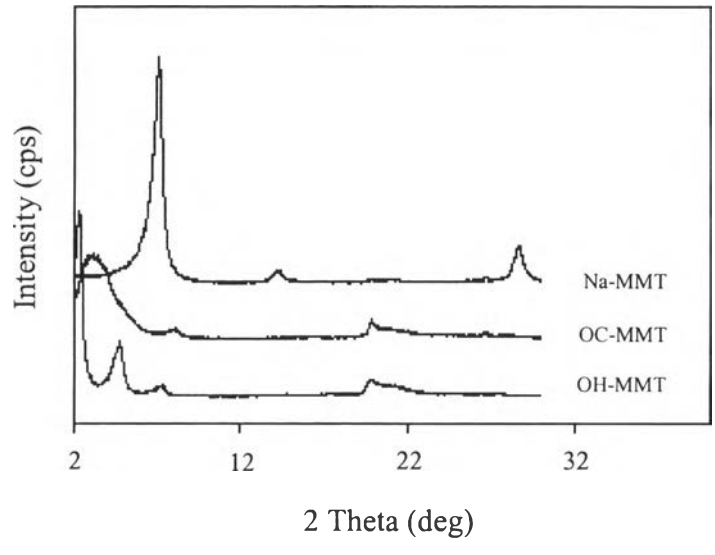

Figure 4.3 XRD spectra of Na-MMT, OC-MMT and OH-MMT.

Table 4.2 Basal spacings of Na-MMT and organically modified MMTs

MMTs	Basal spacing (Å)
Na-MMT	12.40
OC-MMT	26.91
OH-MMT	37.40

The results from XRD indicated that basal spacing of Na-MMT obtained from this work was 12.40 Å and which was closed to that reported by

Thaijaroen, (2000), 12.13 Å, and slightly different from Giannelis, (1996), 11.40 Å. After treated with octadecylamine and di(hydrogenated tallow)dimethylammonium chloride, the basal spacing of OC-MMT and OH-MMT was to be 26.91 Å and 37.40 Å, respectively. In general, the higher degree of basal spacing expansion usually resulted in the higher chance of polymer intercalation, which leads to the more possibility of layered-silicate delamination in polymer matrix.

4.1.3 TGA

Thermogravimetric analysis was applied to confirm the incorporation of modifying agents into the MMT structure. Thermograms of modifying agents, Na-MMT and its modified form are shown in Figure 4.4.

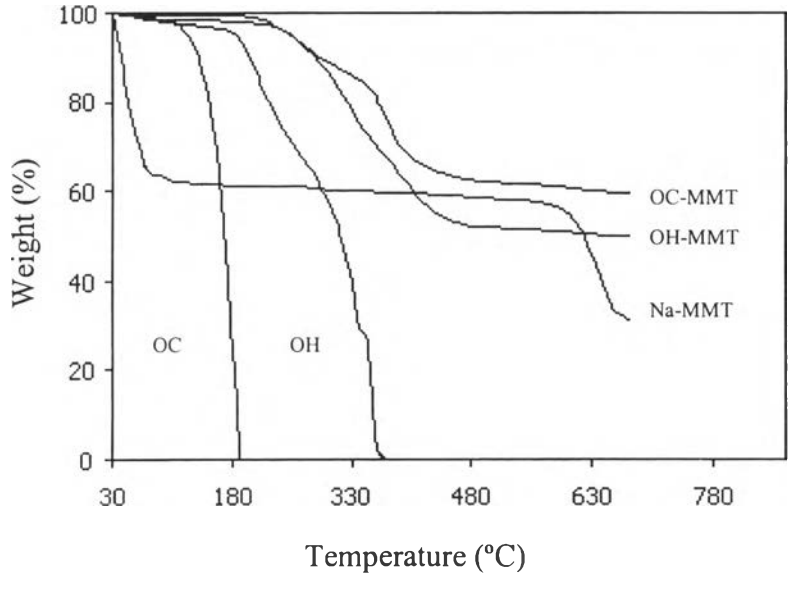

Figure 4.4 TGA thermograms of Na-MMT, OC, OC-MMT, OH and OH-MMT.

The decomposition temperatures (T_d) judged by derivative of modifying agents, OC and OH, are around 180 and 300°C, respectively while that of Na-MMT is around 630°C. The improvement in thermal stability of modifying agents incorporated in MMT structure could be substantiated by the thermogram of OC-MMT and OH-MMT, which showed T_d at 373 and 335°C, respectively.

4.2 Characterization of PEO/MMT Nanocomposites

PEO/MMT nanocomposites with various compositions were characterized using XRD.

4.2.1 Characterization of PEO/Na-MMT Nanocomposites

The obtained PEO/Na-MMT nanocomposites prepared by melt technique were characterized by XRD. It could be clearly observed from Figure 4.5 that the XRD spectra of PEO/Na-MMT nanocomposites prepared by melt technique showed the shift in peak position of Na-MMT from around 7.1 degree (12.40 Å) to 6.0-5.4 degree (14.71-16.35 Å) for every ratio. The results suggested that by mixing PEO with Na-MMT in the pristine form, the distance between silicate layers of Na-MMT would be increased. As a consequent, intercalated nanocomposites of Na-MMT and PEO could be generated by the melt technique. On the other hand, crystalline peaks of PEO are diminished as Na-MMT content increases indicating that Na-MMT acts to inhibit the formation of crystalline structure.

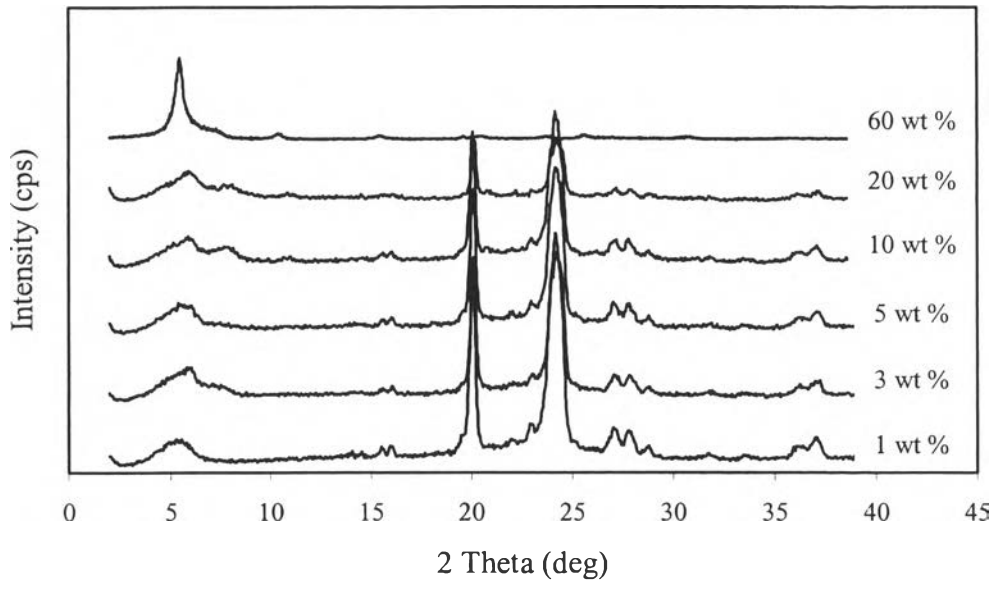

Figure 4.5 XRD spectra of PEO/Na-MMT nanocomposites with various amount of Na-MMT.

4.2.2 Characterization of PEO/OC-MMT Nanocomposites

Comparing PEO/OC-MMT with PEO/Na-MMT nanocomposites, the XRD spectra of PEO/OC-MMT nanocomposites are shown in Figure 4.6.

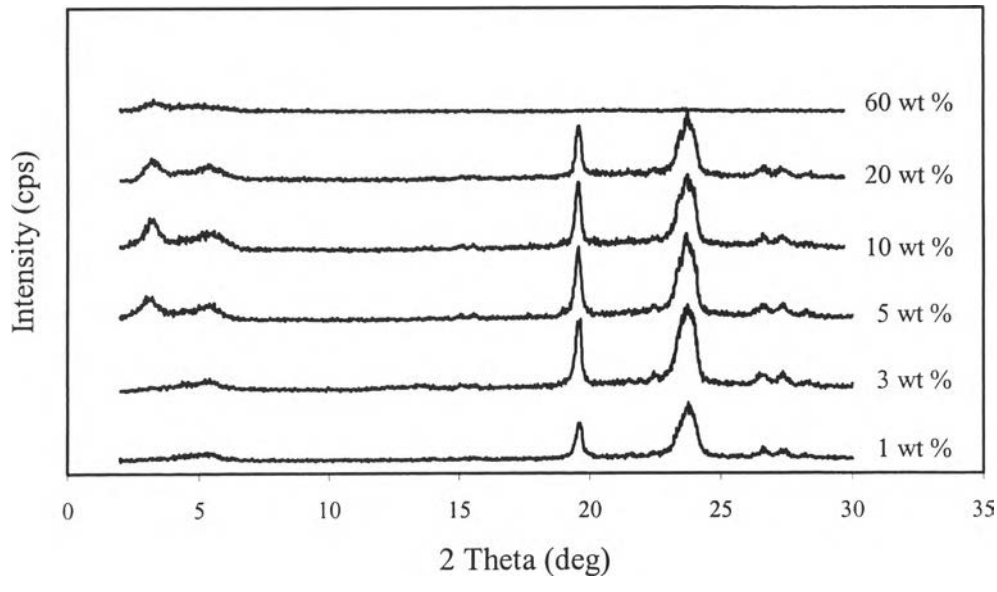

Figure 4.6 XRD spectra of PEO/OC-MMT nanocomposites with various amount of OC-MMT.

For PEO/OC-MMT nanocomposites, the results were different from nanocomposites using Na-MMT. It could be observed that at lower amount of OC-MMT (< 5 wt%), there was no peak presented in the position of OC-MMT. This indicated that silicate layers of OC-MMT were separated into individual layer and relatively far from each other due to the insertion of large amount of PEO. Consequently, exfoliated nanocomposites could be generated. In contrast, for higher amount of OC-MMT, the slightly shift in peak position of OC-MMT to lower degree could be occurred from 3.36 degree (26.27Å) to 3.32-2.96 degree (26.59-29.82 Å). This suggested that among these ratios, intercalated nanocomposites were dominated. At 60 wt% OC-MMT, however, the exfoliation was generated. This corresponds to the disappearance of PEO crystalline structure such that the layer silicate has better chance and less constraint to exfoliate in amorphous matrix. This could be confirmed by TEM of microtomed thin sections as shown in Figure 4.7.

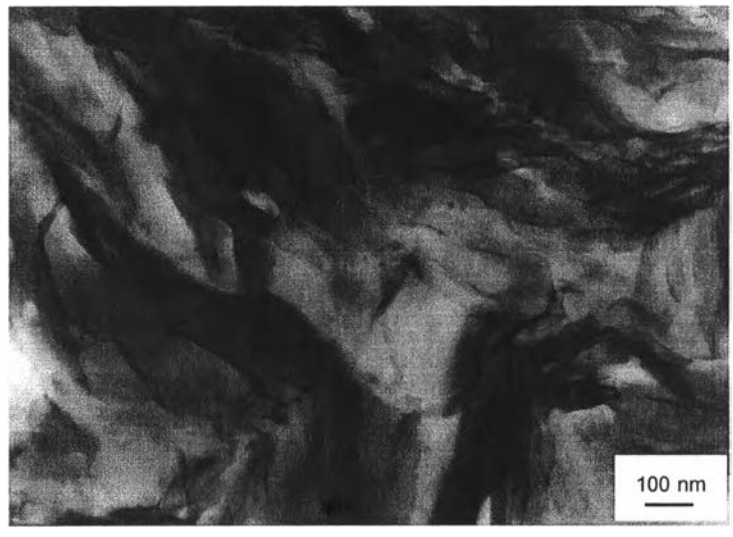

Figure 4.7 TEM micrograph of PEO/OC-MMT nanocomposite containing 60 wt% OC-MMT (× 45,000).

The exfoliation of PEO/OC-MMT nanocomposite containing 60 wt% OC-MMT might be explained by the higher degree of basal spacing expansion (OC-MMT, 14.51 Å), the higher possibility of insertion of PEO. In addition, the larger amount of OC-MMT (more organic-like) provides higher miscibility with PEO matrix.

4.2.3 Characterization of PEO/OH-MMT Nanocomposites

As well as PEO/OC-MMT nanocomposites, PEO/OH-MMT nanocomposites showed similar trend to that of PEO/OC-MMT as shown in Figure 4.8.

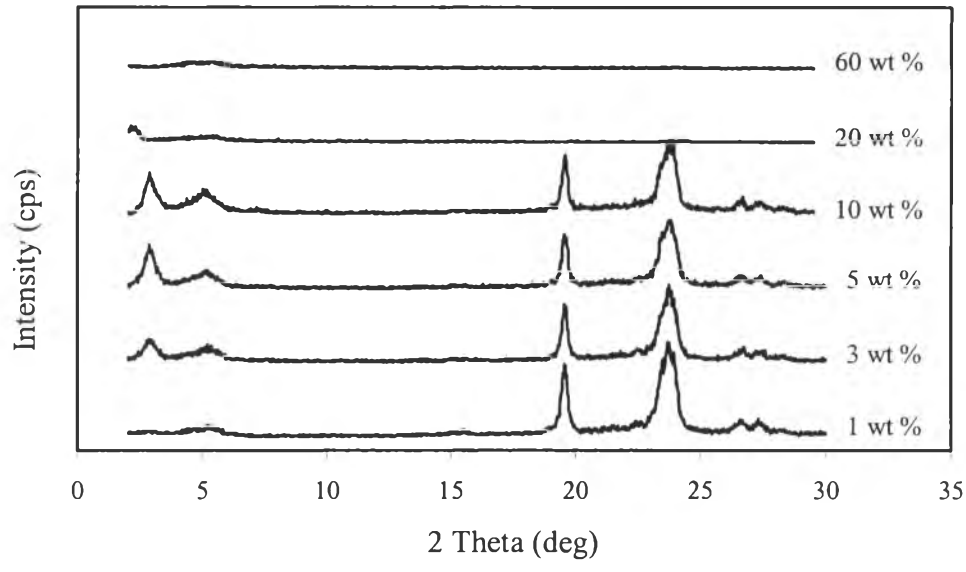

Figure 4.8 XRD spectra of PEO/OH-MMT nanocomposites with various amount of OH-MMT.

4.3 Physical Behavior of PEO/MMT Nanocomposites in Aqueous Solution

Before using the obtained nanocomposites in application for wastewater treatment, the nanocomposites in aqueous solution were studied to observe the physical behavior of them under water condition at constant temperature. In addition, the effect of salt against the physical behavior was also studied.

4.3.1 PEO/Na-MMT Nanocomposites in Aqueous Solution

Light scattering technique was used for structure analysis of macroscopic soluble aggregates by determining particle size of the nanocomposites. Figure 4.9 demonstrates the particle sizes of PEO/Na-MMT nanocomposites in salt-free aqueous solution at various concentrations. It could be seen that for pure PEO, the particle size increases with concentration 0.05g/100ml and then decreases at 0.10g/100ml. This optimum was the result from constraint in expansion of PEO molecules at higher concentration. However, in the presence of Na-MMT, the results show that the particle sizes of PEO/Na-MMT nanocomposites increase as a function of Na-MMT loading.

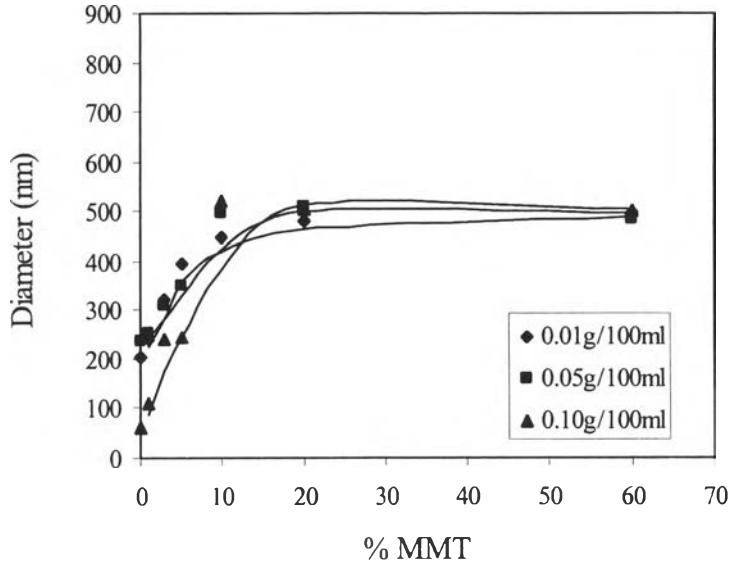

Figure 4.9 Particle size of PEO/Na-MMT nanocomposites in salt-free aqueous solution.

This is the result from the presence of stiff plate-like particles of Na-MMT in the nanocomposites. In addition, the mobilization of Na^+ on the surface of Na-MMT may occur and lead to repulsion of negative charges of PEO and MMT. Up to a certain limit at 10 wt%, the molecular chain expansion is ceased and the particle size reached to the maximum points. The expansion with %MMT becomes slower at higher solution concentration, which attributes to supply of Na^+ sufficient to maintain the size. It might be said that the maximum perturbation was occurred at 10 wt%. However, when salts were added, the structure of the nanocomposites was disrupted as shown in Figure 4.10. It could be observed that the slope or rate of size growth decrease corresponds to the concentration of NaCl especially at 10 and 20% Na-MMT. This could be explained by the neutralization of the charge of Na^+ and Cl^- to the structure of nanocomposites lead to collapse in particle dimension of the nanocomposites at this composition. In other words, there was an increase in coil density, i.e. the polymer mass per unit volume of the polymer species (Mitchell, 1991), compared to that of the dissolved component. However, with high clay content, Na^+ may acts as a physical binder to form particle aggregation leading to about twice increase in particle size.

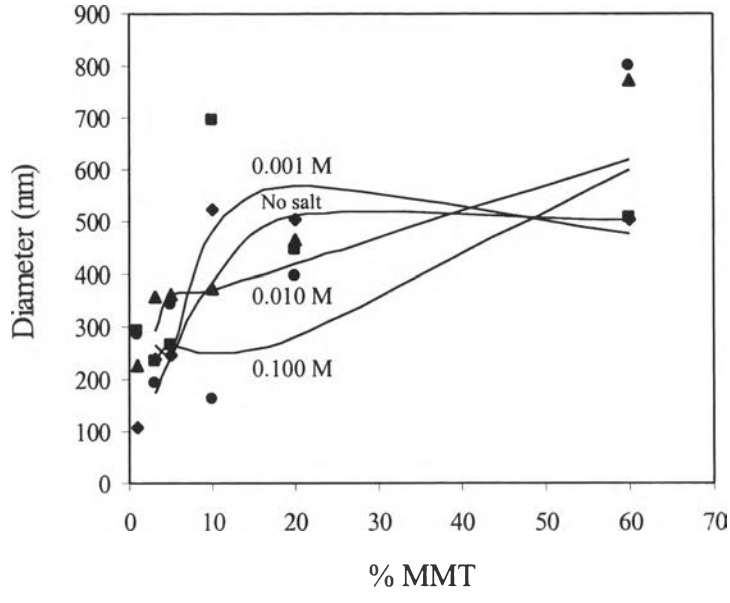

Figure 4.10 Particle size of 0.10 g/100ml PEO/Na-MMT nanocomposites in aqueous solution in the presence of NaCl.

As well as light scattering technique, specific viscosity of the nanocomposites in aqueous solution was also studied. The values are relatively low, about 0.01-0.12. The results show that by increasing concentration, PEO/Na-MMT nanocomposite in aqueous solution shows the decrease of specific viscosity as shown in Figure 4.11. This character could be the result from alignment of PEO molecules under low shear rate condition during viscosity measurement. The specific viscosity increases with nanocomposites concentration despite that the size is decreased. This is due to more number of particles contributes to more hydrodynamic interaction to dissipate energy.

After addition of salts, NaCl, the specific viscosity was diminished down to a minimum corresponding to the decrease in particle size with the concentration of NaCl (Figure 4.12). This behavior could be explained by an increase of coil density as described in particle size measurement. It should be noted here that the viscosity is minimized although the size increases about twice at high concentration and high %MMT. This suggests that this size increment due to loosely bound particles that are disassociated easily under shearing. Therefore, such large aggregate particles do not play role to increase viscosity.

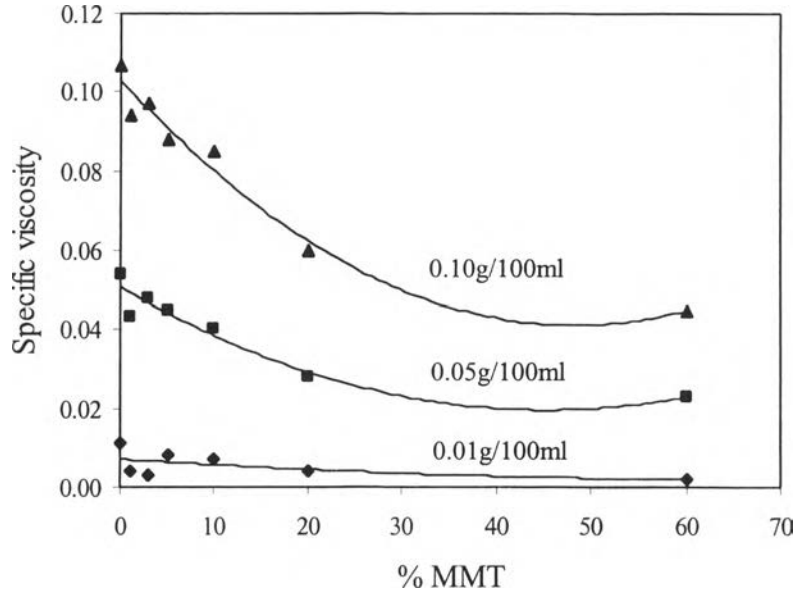

Figure 4.11 Specific viscosity of PEO/Na-MMT nanocomposites in aqueous solution at various concentration.

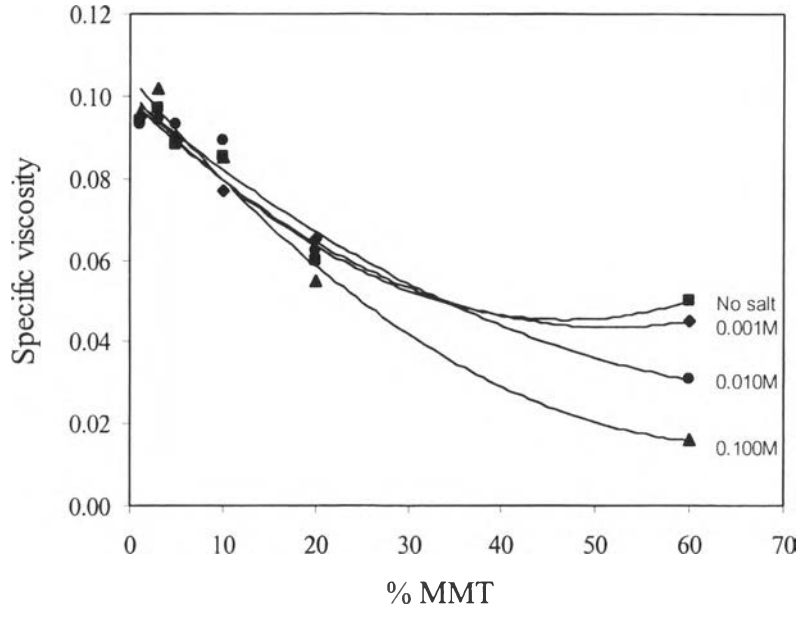

Figure 4.12 Specific viscosity of 0.10g/100ml PEO/Na-MMT nanocomposites in aqueous solution in the presence of NaCl.

4.3.2 PEO/OC-MMT Nanocomposites in Aqueous Solution

The specific viscosity of PEO/OC-MMT nanocomposites in aqueous solution is shown in Figure 4.13. As well as PEO/Na-MMT nanocomposites, the higher the amount of OC-MMT, the lower the specific viscosity at a given

concentration. However, the nanocomposites of OC-MMT show less decrease in specific viscosity than that of Na-MMT due to less effectiveness of OC to increase coil density (octadecylammonium ion has layer size and less polarity than Na^+).

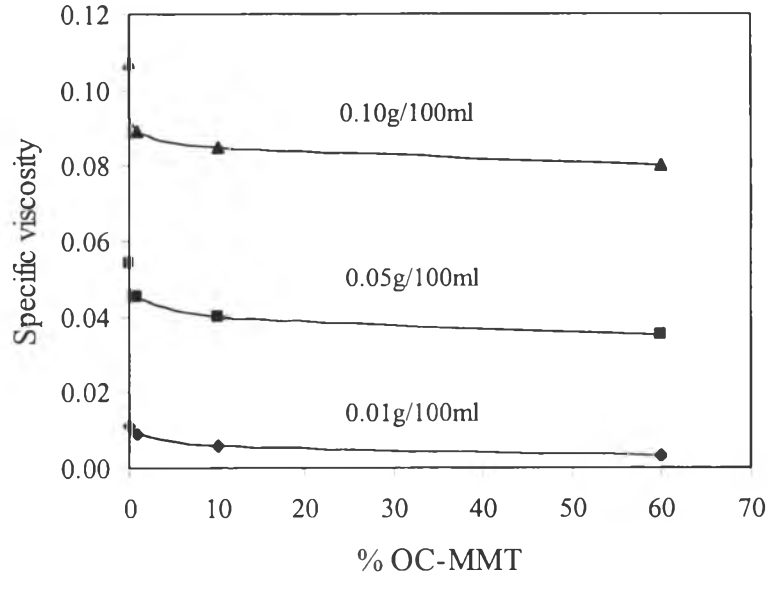

Figure 4.13 Specific viscosity of PEO/OC-MMT nanocomposites in aqueous solution at various concentration.

From the results, it could be indicated that PEO/OC-MMT nanocomposites in aqueous solution also behave like a symplex system, i.e. the decrease in the specific viscosity with minor phase. Moreover, in the presence of NaCl, the specific viscosity of 0.10g/100ml PEO/OC-MMT nanocomposites was decreased at 0.01 M and increase at 0.10 M NaCl (see Figure 4.14). Increasing NaCl content attributes to increasing positive charge to reduce repulsive force so that viscosity decrease. Adding more salt may not be necessary and may lead to the repulsion between Na^+ and octadecylammonium ion resulting in increasing viscosity.

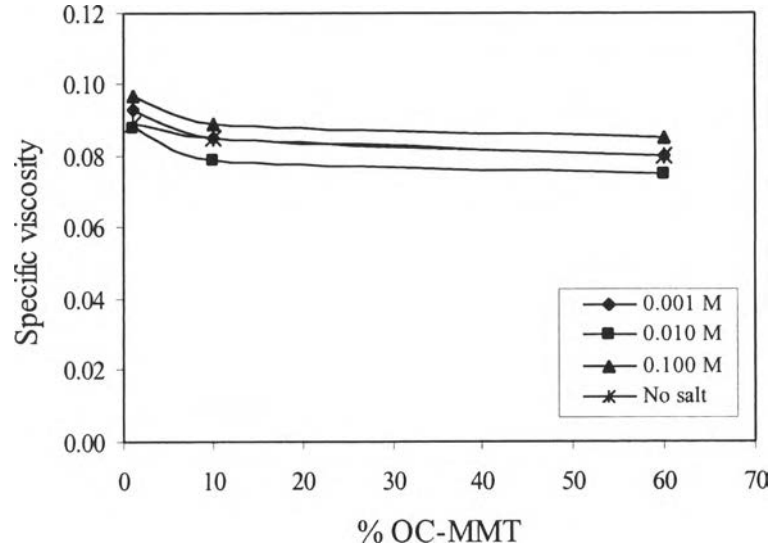

Figure 4.14 Specific viscosity of 0.10g/100ml PEO/OC-MMT nanocomposites in aqueous solution in the presence of NaCl.

4.3.3 PEO/OH-MMT Nanocomposites in Aqueous Solution

PEO/OH-MMT nanocomposites in aqueous solution was relatively similar to PEO/OC-MMT nanocomposites except after addition of salt, the specific viscosity was increased (see Figure 4.15 and Figure 4.16).

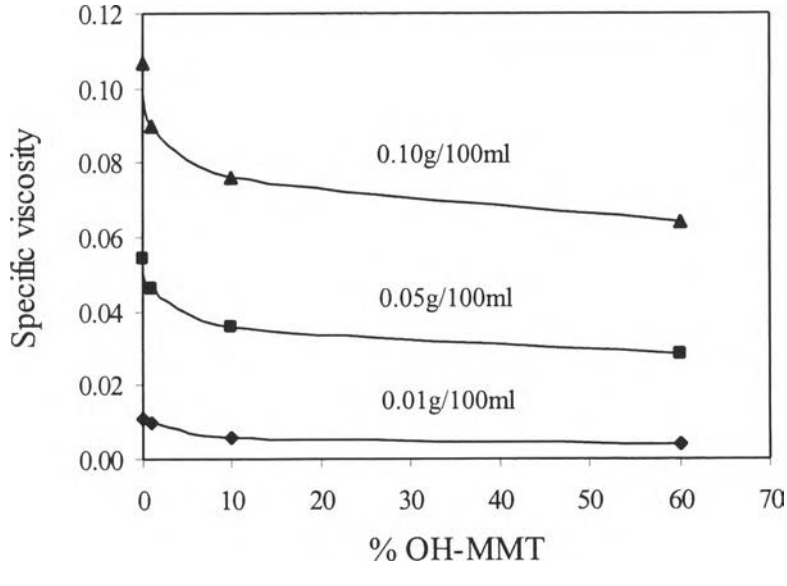

Figure 4.15 Specific viscosity of PEO/OH-MMT nanocomposites in aqueous solution at various concentration.

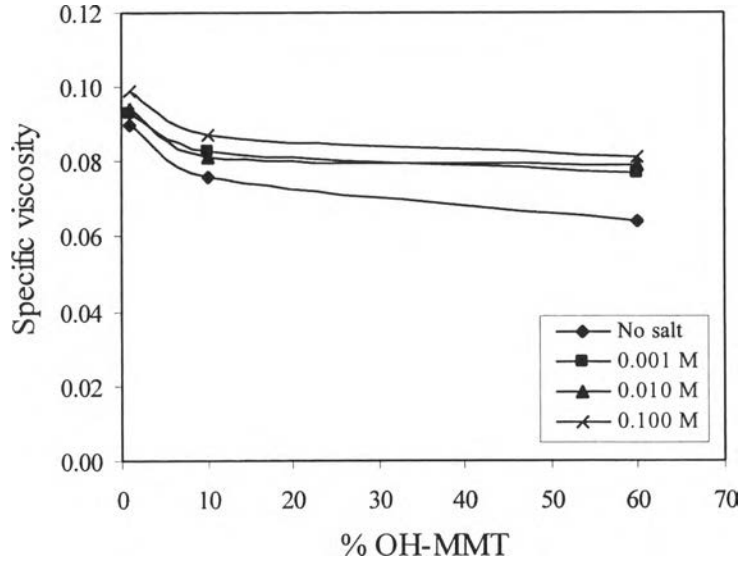

Figure 4.16 Specific viscosity of 0.10g/100ml PEO/OH-MMT nanocomposites in aqueous solution in the presence of NaCl.

OH-MMT is more polar than OC-MMT and more bulky that both OC-MMT and Na^+. It can form hydrogen bonding with PEO leading to lower viscosity. The increase in specific viscosity of PEO/OH-MMT nanocomposites in aqueous solution in the presence of NaCl may be due to the disruption of hydrogen bond and the repulsion of positive charges of tallow quarternary ammonium ion in the nanocomposites.

4.4 Characterization of PAMAM/MMT Nanocomposites

4.4.1 XRD

The XRD spectra of PAMAM/MMT nanocomposites with 10 wt% MMTs are shown in Figure 4.17. It could be observed that the corresponding peaks of Na-MMT, OC-MMT and OH-MMT were disappeared and exfoliation was confirmed to dominate.

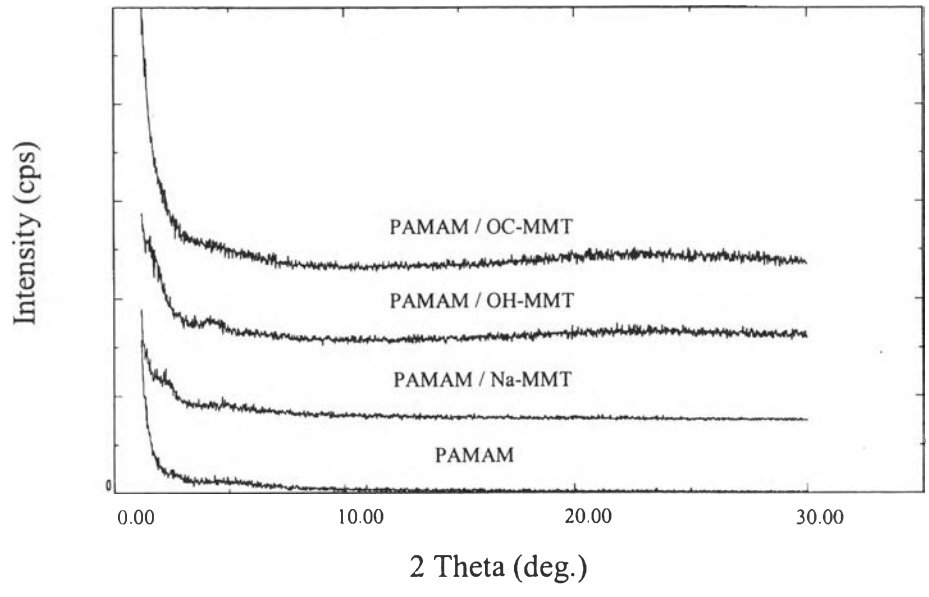

Figure 4.17 XRD spectra of PAMAM/Na-MMT, PAMAM/OC-MMT and PAMAM/OH-MMT nanocomposites containing 10 wt% MMTs.

4.4.2 FT-IR

FT-IR spectra were used to confirm the incorporation of PAMAM into the galleries of the clay. For PAMAM, the spectra showed the important adsorption peaks of N-H stretching of primary amine, C-H stretching of methylene group in alkanes and N-H stretching and C=O stretching of secondary amide at 3293, 2946, 1639 and 1561 cm^{-1}, respectively. All spectra of the nanocomposites, PAMAM/Na-MMT, PAMAM/OC-MMT and PAMAM/OH-MMT, show characteristic peaks of both clay and PAMAM (see Figure 4.18, 4.19 and 4.20).

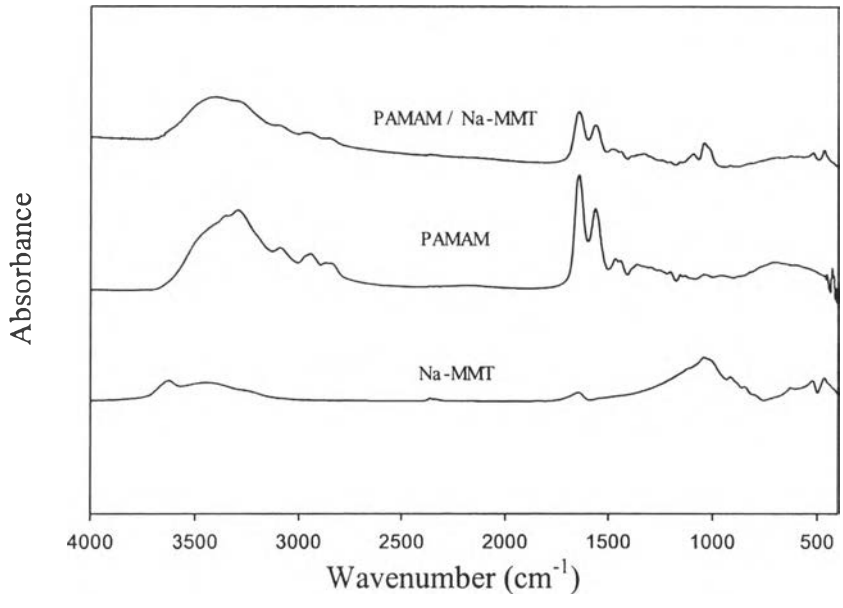

Figure 4.18 FT-IR spectra of Na-MMT, PAMAM and PAMAM/Na-MMT nanocomposite.

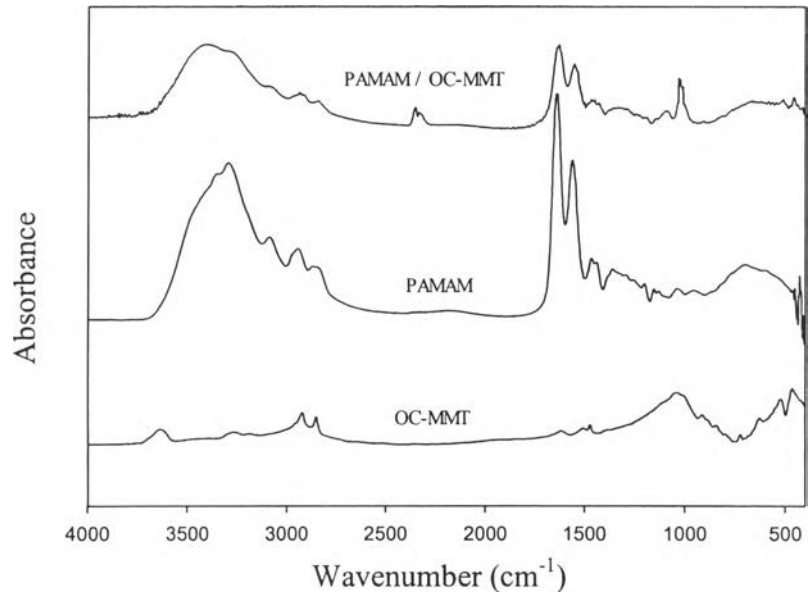

Figure 4.19 FT-IR spectra of OC-MMT, PAMAM and PAMAM/OC-MMT nanocomposite.

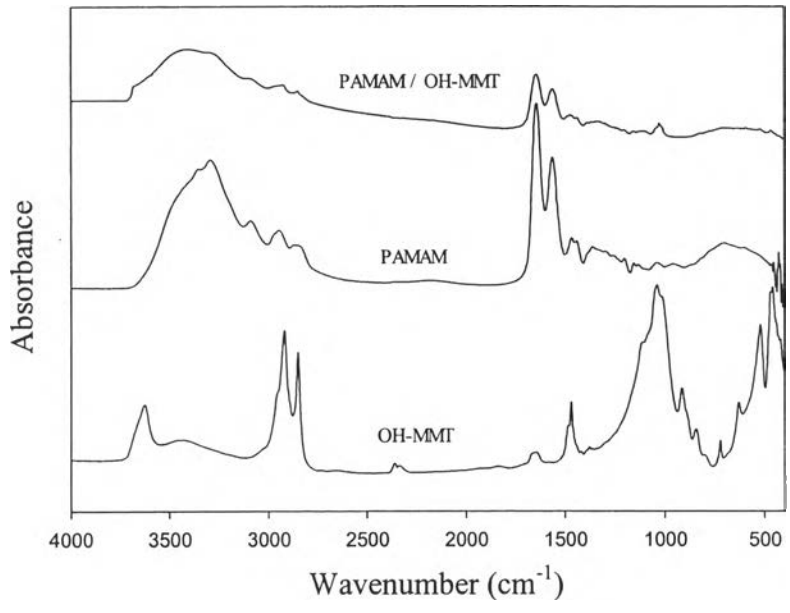

Figure 4.20 FT-IR spectra of OH-MMT, PAMAM and PAMAM/OH-MMT nanocomposite.

4.5 Adsorption Test

4.5.1 PEO/MMT Nanocomposites

4.5.1.1 Toluene Adsorption

Figure 4.21 shows the amount of toluene adsorbed onto the PEO/Na-MMT, PEO/OC-MMT and PEO/OH-MMT nanocomposites at various compositions. It is seen that the ability to adsorb toluene is enhanced by the increase in amount of OC-MMT and OH-MMT in the nanocomposites. In case of OC-MMT, the introduction of long alkyl chains to the structure of MMT improved the toluene adsorption ability. For OH-MMT, it has been reported that the modified MMT with quaternary ammonium cation could improve the sorbent property of MMT for organic molecules (Wibulswas, 2000). Contrary to PEO/Na-MMT nanocomposite systems, the inorganic exchangeable cations (Na^+) between the layer of MMT are strongly hydrated by water. Consequently, the adsorption of nonionic organic compounds (NOCs), such as benzene, alkylbenzenes and chlorinated phenols

(Kukkadapu and Boyd, 1995), by MMT is reduced in the presence of water because NOCs cannot effectively compete with highly polar water molecules for adsorption sites on the MMT surface (see Figure 4.22). Therefore, increasing in amount of Na-MMT led to decrease in ability of the nanocomposite to adsorb toluene.

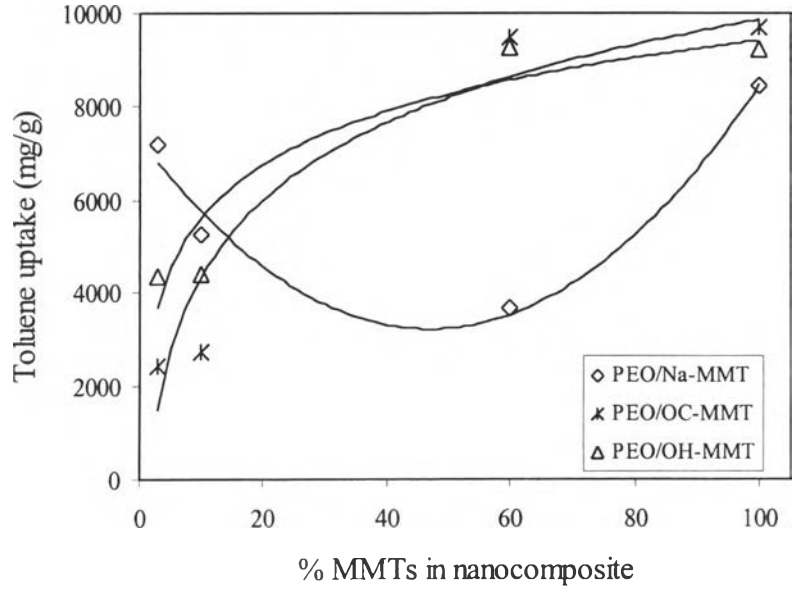

Figure 4.21 Amount of toluene adsorb onto nanocomposites at various compositions (initial toluene concentration 86.7 mg/ml at constant concentration of nanocomposite 0.1g/100ml).

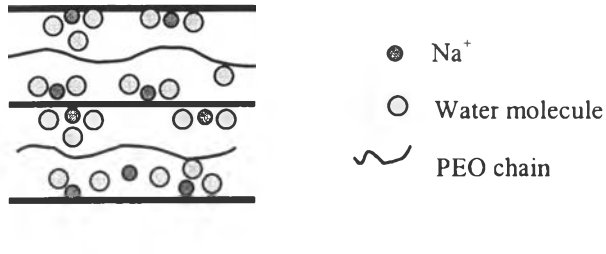

Figure 4.22 Schematic illustration of hydrated Na^+ by water in PEO/Na-MMT nanocomposite.

In this case, PEO/OH-MMT nanocomposites is more effective to adsorb toluene than PEO/OC-MMT nanocomposites. However, at 100% Na-MMT, the adsorption becomes the highest. This might be explained that at this composition, there is no effect of bridging flocculation (Swenson, 2001). This effect

is occurred by the presence of high-molecular-weight polymer (PEO) which supposes that the two ends of a PEO chain adsorb onto both MMT surfaces and thereby draw them together and induces a reduction of the interlayer spacing results in the reduction of adsorption of toluene (see Figure 4.23). Moreover, Na-MMT has high degree of swelling in water that could be lead to higher adsorption of toluene.

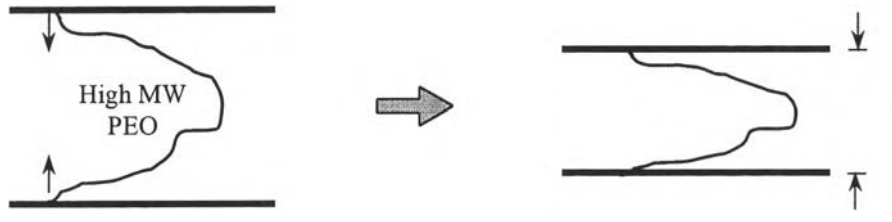

Figure 4.23 Schematic illustration of bridging flocculation occurs in polymer nanocomposite in the presence of high molecular weight polymer.

4.5.1.2 Xylene Adsorption

The results from xylene adsorption were relatively similar to that of toluene as shown in Figure 4.24. The capacity of xylene adsorbed onto PEO/MMT nanocomposites increases with increasing organoclay and show higher increment than the system of PEO/Na-MMT nanocomposites. This result confirms the proposed concept of using organoclay as an adsorbent for the removal of organic molecules from aqueous solution. The schematic illustrations of toluene and xylene adsorption of PEO/organoclay nanocomposites with high and low percentage of organoclay are shown in Figure 4.25. It is likely that PEO/OH-MMT can adsorb both toluene and xylene better than PEO/OC-MMT regardless of exfoliated or intercalated nanocomposites. Thus, the adsorption can be contributed to comparable polarity of the adsorbent and adsorbate and the gallery spacing (OH-MMT > OC-MMT).

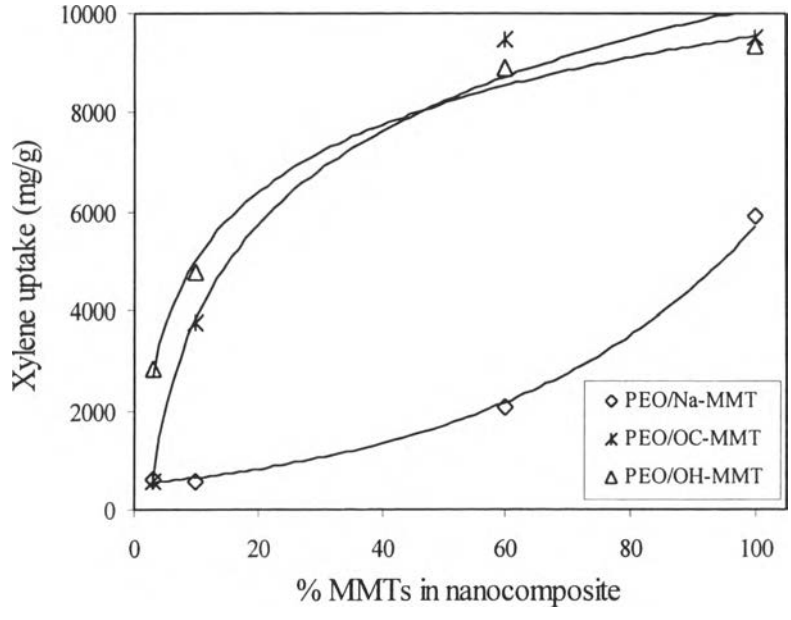

Figure 4.24 Amount of xylene adsorb onto nanocomposites at various compositions (initial xylene concentration 86.0 mg/ml at constant concentration of nanocomposite 0.1g/100ml).

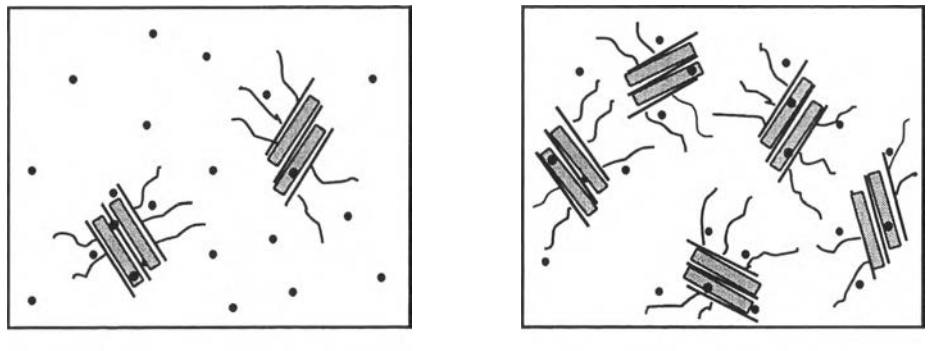

Figure 4.25 Schematic illustration of toluene and xylene adsorption of PEO/organoclay nanocomposites.

4.5.2 PAMAM/MMT Nanocomposites

Figure 4.26 shows the comparison of the ability of toluene and xylene adsorption by PAMAM/MMT nanocomposites containing 10wt% of MMTs.

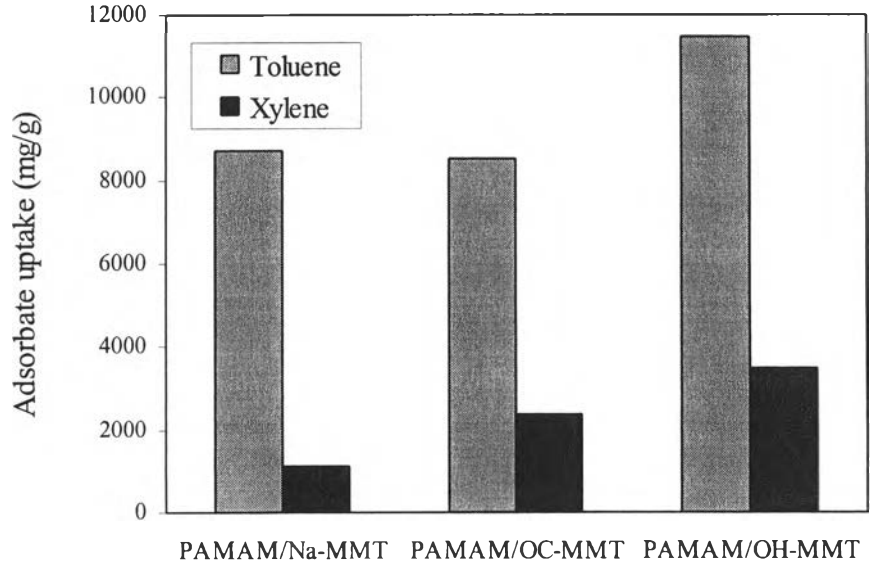

Figure 4.26 Toluene and xylene adsorption of PAMAM/MMT nanocomposites containing 10 wt% MMTs.

It is clearly seen from the figure that the amount of toluene uptake by PAMAM/MMT nanocomposites is much greater than that of xylene for all types of clay. This implies that the nanocomposites of poly(amidoamine) and MMTs have higher affinity for toluene than that of xylene. This can be due to structure hindrance, i.e. two methyl groups on xylene molecules thus may not allow xylene to adsorb well on PAMAM/MMT nanocomposites and more hydrophobicity of xylene than toluene.

The efficiency of the adsorbent PAMAM/MMT nanocomposites are compared with PEO/MMT nanocomposites in aqueous system as shown in Figure 4.27. It could be seen that PAMAM/MMT nanocomposites show much higher toluene adsorption than that of PEO/MMT nanocomposites for all types of MMT.

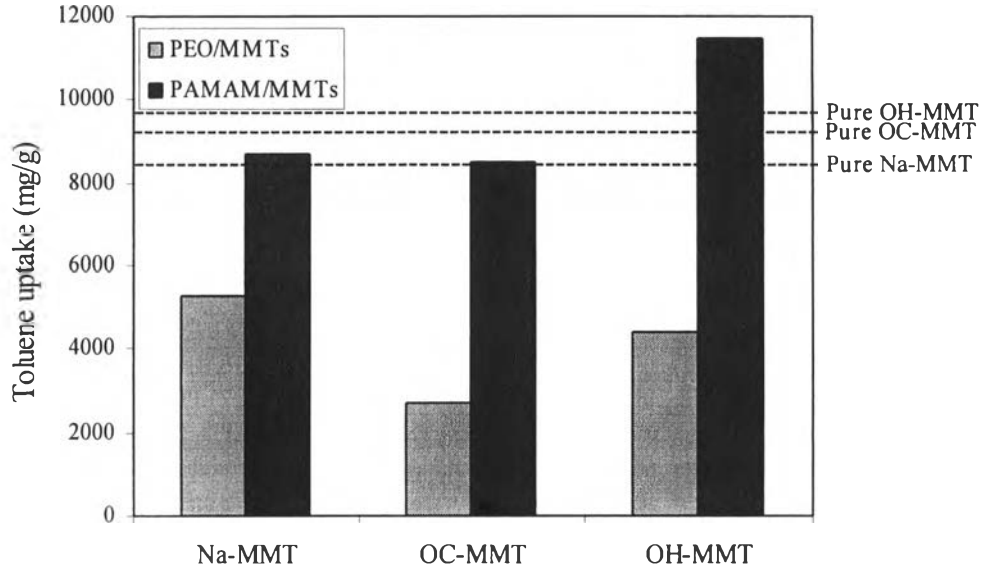

Figure 4.27 Toluene adsorption of PEO/MMTs and PAMAM/MMT nanocomposites containing 10 wt% MMTs.

The higher efficiency of PAMAM/MMT nanocomposites as an adsorbent for organic solvent, i.e. toluene and xylene, is due to the structure of second generation PAMAM with highly branching alkyl chains that could improve the affinity for toluene. In addition, bulky molecules of PAMAM incorporated to MMTs structure provided higher d-spacing (or exfoliation) than PEO/MMT nanocomposites that result in higher ability for adsorption.

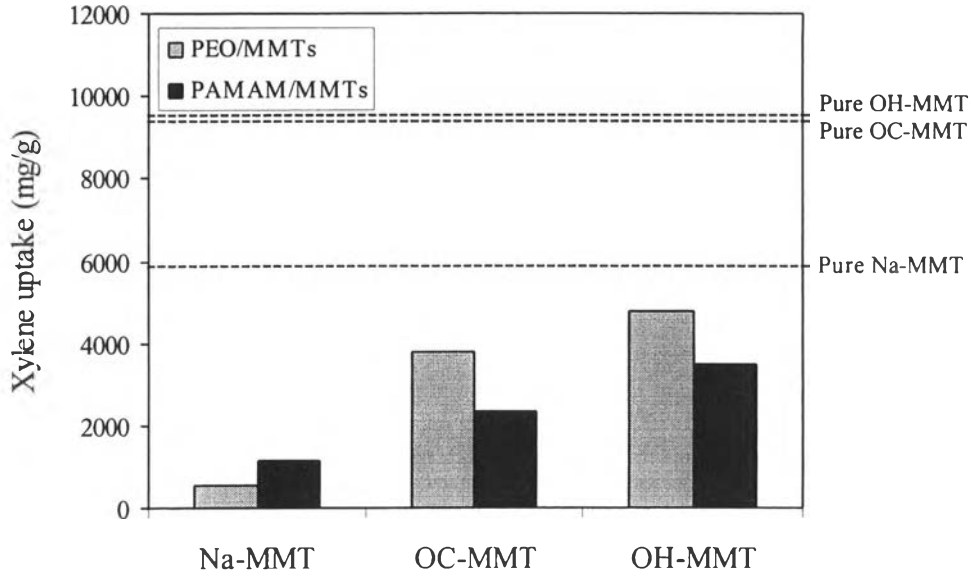

Figure 4.28 Xylene adsorption of PEO/MMTs and PAMAM/MMT nanocomposites containing 10 wt% MMTs.

However, this characteristic was not observed in the case of xylene adsorption. PEO/OC-MMT and PEO/OH-MMT nanocomposites showed higher efficiency for xylene adsorption than PAMAM/MMT nanocomposites because of the lower in polarity of xylene than that of toluene. OC-MMT is poorer than OH-MMT nanocomposites due to more hydrophobicity or less polarity of octadecylamine (aliphatic amine) compared to the adsorbate (aromatic). This could be implied that PAMAM/MMT nanocomposites at 10 wt% MMTs have a degree of selectivity for toluene and xylene.